JOURNAL OF MATERIALS SCIENCE **36** (2001) 1173–1182

The influence of electrodes on the strength of planar zirconia solid oxide fuel cells

A. SELÇUK, G. MERERE, A. ATKINSON
Department of Materials, Imperial College, London SW7 2BP, UK
E-mail: alan.atkinson@ic.ac.uk

The strength of symmetric anode/electrolyte/anode and cathode/electrolyte/cathode planar multiple electrode assemblies (MEAs), fabricated by screen printing electrodes onto pre-fired tape-cast electrolyte plates was measured in biaxial flexure. The electrolyte was $Zr_{0.84}Y_{0.16}O_{1.92}$ (YSZ), the anode NiO/YSZ and the cathode $La_{0.75}Sr_{0.2}MnO_{3-\delta}$. The residual stress in the electrodes was estimated by curvature measurement after removal of one electrode. The residual stress in the anodes was very low (11 MPa) due to stress relief by extensive channel cracking. The residual stress in the cathodes was much higher (39 MPa) and was in reasonable agreement with the expected thermoelastic stress. The applied load at failure, and the stress in the electrolyte at failure (343 MPa), for anode MEAs were almost equal to those of electrolyte plates (374 MPa). This is consistent with the low residual stress and observed crack deflection by delamination at the anode/electrolyte interface. The applied load at failure, and the stress in the electrolyte at failure (182 MPa), for cathode MEAs were much lower. This is partially explained by the residual stress in the cathode acting to increase the applied stress intensity at defects in the electrolyte, but this effect is not large enough to explain fully the reduced strength.

1. Introduction

The mechanical properties of the ceramic components are particularly important for ensuring the reliability of solid oxide fuel cells (SOFC) and other similar devices based on dense ceramic ion-conducting membranes. In planar SOFCs, with a self-supporting electrolyte, the electrolyte membrane and its cathode and anode electrodes (called the multiple electrode assembly, or MEA) is a critical mechanical component of the fuel cell stack. The compromise between high mechanical strength and low electrical resistance results in a rather fragile MEA having the lowest thickness consistent with acceptable mechanical strength. In previous work [1–4] we have reported on the mechanical properties of the individual materials that constitute the MEAs for SOFCs operating at relatively high temperatures (800 to 1000°C). These are: dense zirconia stabilised with 8 mole % yttria, $Zr_{0.84}Y_{0.16}O_{1.92}$ (YSZ) as electrolyte; porous $La_{1-x}Sr_xMnO_3$ (LSM) cathode; and two-phase NiO/YSZ (75mol % NiO/25 mol % YSZ) precursor to the Ni/YSZ cermet anode. These materials were all studied in the form of thin sheets produced either by tape casting or a proprietary polymer vehicle film stretching process (Solufil).

During the production of MEAs it had been observed that they were weaker than anticipated from the known properties of the constituent materials. The objective of the work described here was to establish the effect of the anode and cathode individually on the strength of symmetrical MEAs and to understand the mechanism responsible for weakening.

2. Experiments

2.1. Specimen fabrication

The YSZ electrolyte membranes were square sheets with nominal final dimensions of $5 \times 5 \times 0.15$ mm produced by tape casting and sintered at 1500°C to >98% theoretical density. The electrodes were applied by screen printing onto the sintered electrolyte and fired at 1300°C. The electroded specimens were symmetrical in that the same electrode was applied to both sides of the electrolyte. The LSM cathodes ($La_{0.75}Sr_{0.2}MnO_{3-\delta}$) were applied as powder admixed with carbon black, which burned out during firing and acted as a pore former. The nominal fired thickness of the cathodes was 25 μm. The porosity of the cathodes was determined from the mass and dimensions of the final specimens to be ~35%. The symmetrical specimens with anodes were prepared in a similar way and tested in the oxidised intermediate state (i.e. with NiO rather than the metallic Ni of the working anode). The volume fraction of porosity in the oxidised anodes was measured to be ~32% and their nominal thickness was 35 μm.

2.2. Residual stress

Since the MEAs studied here are symmetrical, the residual stresses do not cause any bending of the laminates.

Therefore the residual stresses were obtained by observing the bending after one of the electrodes had been removed. This allows the average stress in the electrode to be determined. As-fabricated symmetrical MEAs were first cut into four smaller specimens (approximately 20 × 20 mm) using a diamond scriber. The anodes were found to be only weakly bonded to the electrolyte and were easily removed using silicon carbide paper. The cathodes were more strongly bonded, but could be removed using a steel razor blade. The surface profiles of the specimens were measured in two orthogonal directions on the exposed electrolyte surface over the full width of the specimen using a Talysurf profiler (Taylor-Hobson).

Initial experiments revealed that the YSZ itself was not flat and therefore a method was devised to take this into account. This was done by measuring the surface profile of each specimen with one electrode removed and then measuring it again after removal of the second electrode. The profile obtained from the specimen with both electrodes removed was subtracted from that measured on the same specimen with only one electrode removed in order to obtain the distortion caused by the residual stress in the electrode. Typical examples of the measured profiles and the corresponding ones corrected for the distortion of the YSZ are shown in Fig. 1. In order to determine the specimen curvature, the corrected profiles were fitted to the arc of a circle by adjusting the radius and centre of the circle in order to minimise the standard error. Examples of the corrected and fitted profiles are shown in Fig. 2. The residual stresses in the single electrode and double electrode specimens were estimated from the theory of bending of thin shells [5].

2.3. Biaxial flexure strength

Biaxial flexure strength of the 50 × 50 mm square plates of MEAs was measured in the ring-on-ring configuration [3] with an outer supporting ring of radius 19 mm and an inner loading ring of radius 4.75 mm. The loading jig was constructed from hardened steel and the radius of curvature of the loading rings was 1 mm. The load was applied at a crosshead displacement rate of 2 mm per minute. Similar measurements were also made on specimens of YSZ electrolyte that had not had any electrodes applied. Ten specimens were tested from each batch in order to obtain reasonable statistical significance.

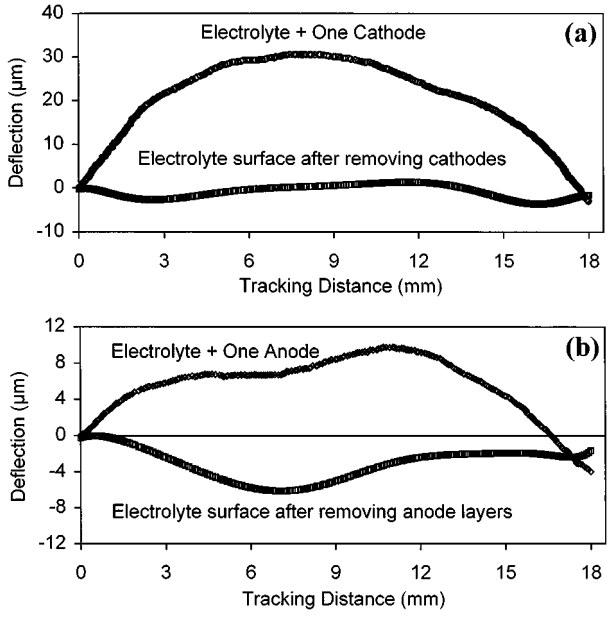

Figure 1 Surface profiles of (a) a cathode MEA and (b) an anode MEA showing the surface profile for the YSZ (electrodes removed) and the surface profile for the same specimen with only one electrode removed.

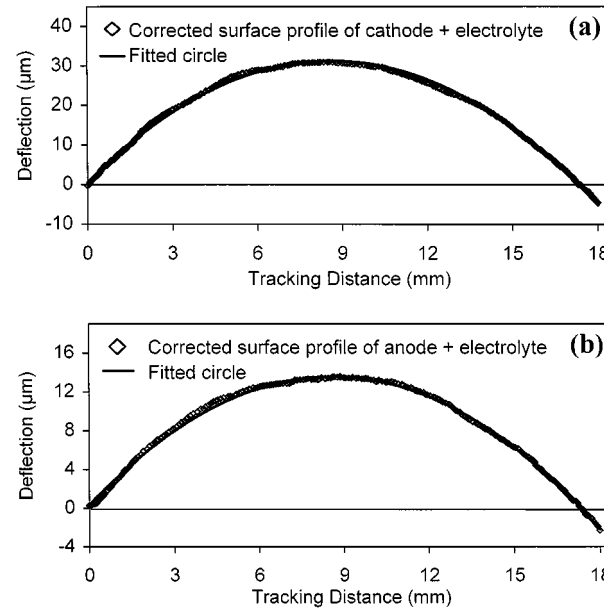

Figure 2 Corrected measured surface profiles of; (a) a cathode MEA and (b) an anode MEA, with one electrode removed and fitted to circular profiles.

The stress at failure was calculated using finite element modelling (FEM) to take into account the non-linear relationship between load and displacement that arises in such a loading geometry. The biaxial flexure of the specimen was simulated using the three dimensional shell elements available in the ABAQUS code (Version 5.7) and assuming friction-less loading. The principal stresses, σ_{11} and σ_{22}, obtained from the FEM solutions, were used to determine the radial (biaxial) stresses, σ_b, according to the relationship

$$\sigma_b = \sigma_{11}\,\mathrm{Cos}^2\theta + \sigma_{22}\,\mathrm{Sin}^2\theta \qquad (1)$$

where θ is the angle between the radial direction and the σ_{11} direction at any point on the specimen. Thus, the biaxial stress distribution throughout the specimen was analysed as a function of the applied load. The fracture of the single-layer YSZ electrolyte specimens was found to initiate at or within the loading ring area. The FEM results also indicated that the stresses are maximised within the loading circle on the tensile surface of the specimens. Therefore the fracture stress of these specimens is quoted here as the maximum tensile stress which developed within the loading circle at fracture. When modelling the flexural behaviour of the three-layer MEAs, the measured residual stresses in the MEAs were incorporated as a separate step in the model before calculating the total biaxial flexure

stresses. The cross-sectional distribution of the total stresses determined after the biaxial loading indicated that the stresses are maximised within the loading circle on the YSZ side of the electrode-YSZ interface where the applied load induces tensile stresses. The fracture stress of MEAs was taken as the maximum tensile stress which developed at fracture within the loading circle on the YSZ side of the interface.

2.4. Dilatometry

In order to interpret the residual stresses, it is necessary to have accurate data for the difference in thermal expansion between the electrode and electrolyte layers. Therefore, the thermal expansions of YSZ, LSM and NiO-YSZ were measured using bars of these materials ($5 \times 5 \times 25$ mm^3) with microstructural features, such as porosity and grain size, which were similar to those of the layers in MEAs. Measurements were carried out in air in the temperature range from 25°C to 1500°C for the YSZ electrolyte and to 1300°C for the electrodes using a commercial dilatometer calibrated against a sapphire standard specimen. A heating/cooling rate of 3°C per min was applied in all measurements.

2.5. Microstructural characterisation

The planar surfaces of the MEA specimens were examined in a scanning electron microscope (SEM) (Jeol JSM-35) in order to characterise the crack patterns on the electrode surfaces. The fracture surfaces of the specimens tested in biaxial flexure were also examined by SEM in order to determine the typical defects responsible for the fracture of MEAs.

3. Results and discussion

3.1. Residual stresses and electrode cracking

From the surface profile measurements on 3 single electrode specimens of each type the radius of curvature was found to be 1.1 ± 0.04 m for the cathode specimens and 2.96 ± 0.06 m for the anode specimens. This indicates that the residual stress in the cathodes is significantly greater than that in the anodes and the sign of the curvature corresponds to a tensile stress. The residual stress is due to the difference in thermal expansion coefficient between the electrolyte and the electrodes as the MEA is cooled down from the electrode firing temperature. Assuming that all strains are elastic then the total strain is the sum of the thermal expansion mismatch strain and the strain caused by the residual stress. For the three-layer MEAs, which remain flat as a result of their symmetry, the residual stresses are given by

$$\sigma_1 = \frac{(\alpha_2 - \alpha_1)\Delta T}{\frac{1}{\hat{E}_1} + \frac{2h_1}{h_2}\frac{1}{\hat{E}_2}} \quad \text{and} \quad \sigma_2 = \frac{(\alpha_1 - \alpha_2)\Delta T}{\frac{1}{\hat{E}_2} + \frac{h_2}{2h_1}\frac{1}{\hat{E}_1}} \tag{2}$$

where α is thermal expansion coefficient, $\Delta T (= T_i - T_f)$ is the change in temperature from T_i to T_f, h is the layer thickness and $\hat{E}$ is the biaxial modulus given by $\hat{E} = E/(1-\nu)$. The subscripts 1 and 2 refer to the electrolyte and electrode respectively. The effective thermal expansion mismatch strain can be deduced from the measured radius of curvature, r, of the single electrode laminates:

$$(\alpha_2 - \alpha_1)\Delta T = \frac{Ch_2^2}{6r}\left(\frac{1}{h_1} + \frac{1}{h_2}\right) \tag{3}$$

where

$$C = 4 + 6\left(\frac{h_1}{h_2}\right) + 4\left(\frac{h_1}{h_2}\right)^2 + \frac{\hat{E}_2}{\hat{E}_1}\left(\frac{h_2}{h_1}\right) + \frac{\hat{E}_1}{\hat{E}_2}\left(\frac{h_1}{h_2}\right)^3. \tag{4}$$

The elastic and mechanical properties of LSM, YSZ and NiO-YSZ, reported previously [1–4], are given in Table I. The temperature dependence of the thermal expansion of the three materials is described in Table II. Using the data in Tables I and II and Equation 3, the effective value of ΔT for each electrode system was calculated by iteration. Then the stresses in the three-layer MEAs were calculated using the effective values of ΔT in Equation 2.

The effective cooling temperature difference, ΔT, and the corresponding residual stress in the two-electrode symmetrical MEAs are given in Table III. The effective cooling temperature difference for the cathode specimens ($\Delta T = 1050$°C) is close to the real cooling temperature difference ($\Delta T = 1275$°C) and the small difference may be due to some stress relief that occurred during cooling to 1050°C. The residual stress is approximately 38 MPa tensile which is smaller than the measured strength of similar cathodes (Table I).

TABLE I Elastic constants, biaxial flexure strength and thermal expansion coefficient of electrolyte and electrode materials

Material	Porosity (%)	E (GPa)	ν	Mean strength (MPa)
YSZ [3]	<2	215	0.32	377
LSM [1-2]	33	35	0.25	46
NiO-YSZ [1-2]	31	55	0.17	56

TABLE II The thermal expansion coefficients of LSM, YSZ and NiO-YSZ

Material	Thermal expansion coefficients at 1000 °C ($\times 10^{-6}$ K^{-1})	The constants for thermal expansion coefficients (ppm K^{-1}) ($\alpha = AT^6 + BT^5 + CT^4 + DT^3 + ET^2 + FT + G$), T = temperature, °C						
		A $\times 10^{-23}$	B $\times 10^{-20}$	C $\times 10^{-16}$	D $\times 10^{-13}$	E $\times 10^{-11}$	F $\times 10^{-9}$	G $\times 10^{-6}$
YSZ	1.18	1.785	−8.935	1.717	−1.566	6.536	−5.576	7.312
LSM	1.17	3.534	−0.140	2.037	−1.234	1.557	16.32	5.289
NiO-YSZ	1.06	0.915	−4.722	0.915	−0.815	3.027	0.119	0.100

TABLE III Curvature of single electrode bilayers, effective thermal expansion mismatch temperature and estimated residual stresses in two-electrode symmetrical MEAs

Electrode type	Radius of curvature (m)	Effective ΔT (°C)	Residual stress in electrode (MPa)	Residual stress in electrolyte (MPa)
Anode	2.96	70	10.6	−4.0
Cathode	1.11	1010	38.5	−12.9

This implies that the cathode should not crack during cooling from the firing temperature. Indeed, the SEM observations of the cathode surfaces revealed the absence of cracks as shown in Fig. 3a and 3b. The surface defects observed in the form of isolated short cracks (Fig. 3) are known to be induced by sintering shrinkage. Although these defects are separated by at least 500 μm, some limited local stress relief in their surroundings is expected to occur. This might be partly responsible for the lowering of the real ΔT value to

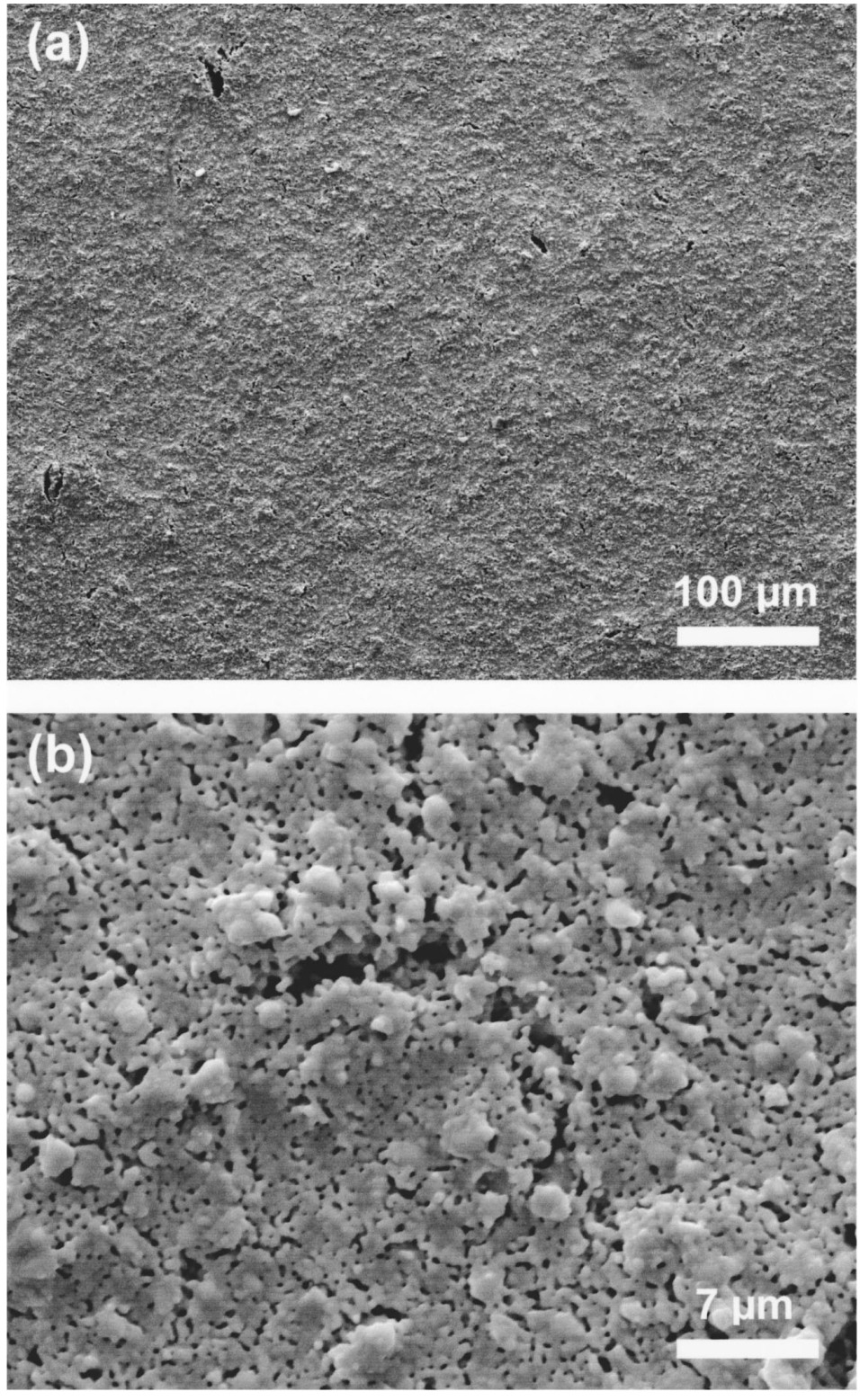

Figure 3 (a) and (b) SEM secondary electron images showing the surface of LSM layer in the three-layer MEAs.

1050°C, but is not extensive enough to cause significant relaxation of the thermal stress.

The value of ΔT for the anode specimens ($\Delta T = 70$°C) is very much lower than the real cooling temperature difference ($\Delta T = 1275$°C). This indicates that most of the thermal expansion mismatch strain has been accommodated by non-elastic deformation in the anodes, such as micro-fracture. This is consistent with the SEM micrographs in Fig. 4a and 4b which show examples of a network of extended cracks in the anode layers. This type of cracking is usually referred to as channel cracking and the cracks interact with each other due to the network they form. From the SEM observation of several surface regions, the crack separation was found to be approximately 200 ± 25 μm.

3.2. Analysis of channel cracks

Several fracture mechanics models for channel cracking of thin films have been proposed in the literature. Analyses of Ye *et al.* [6] and Beuth [7] reveal that the channel cracking of films is a steady-state problem. A crack nucleates from a defect in the film and

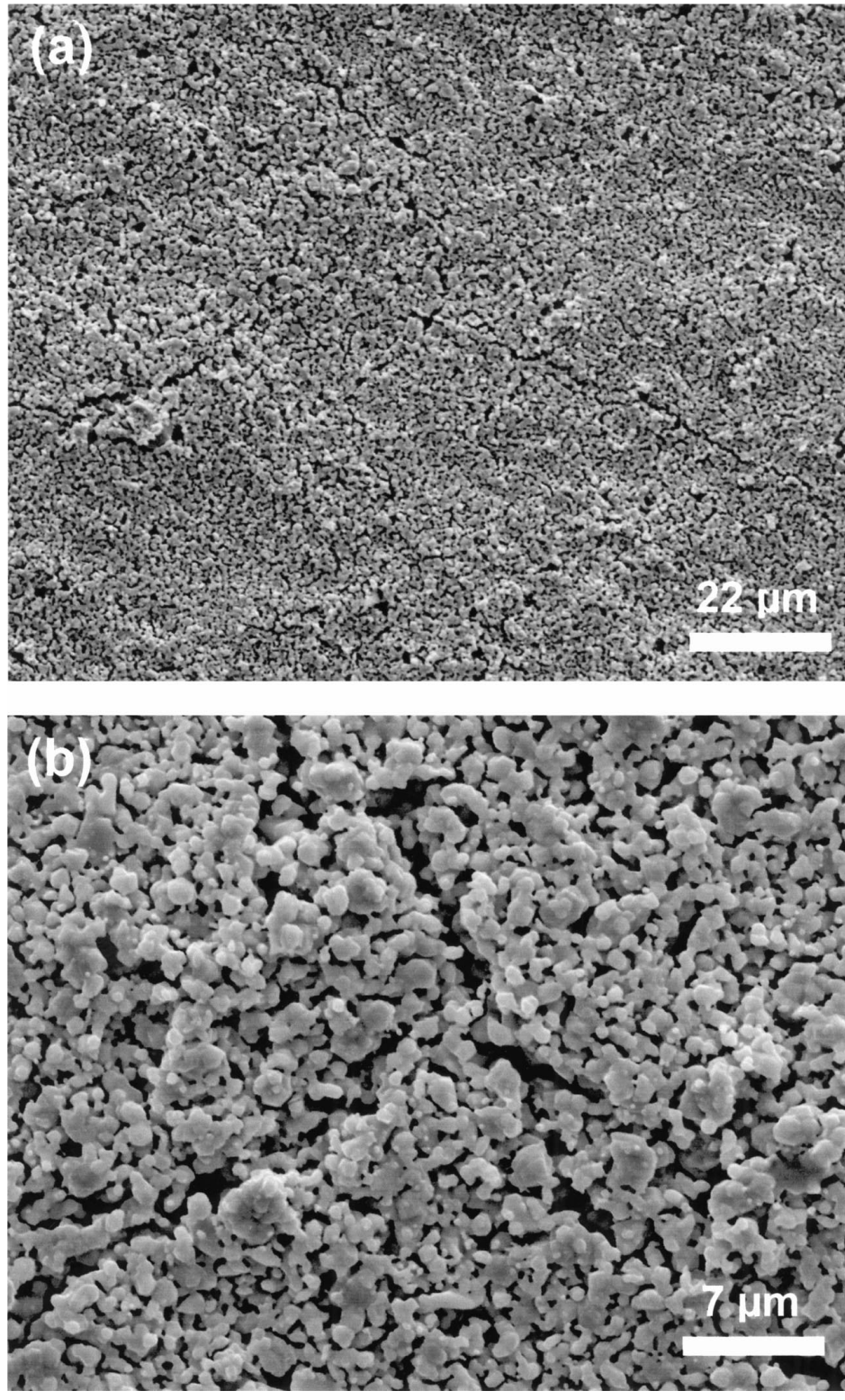

Figure 4 (a) and (b) SEM secondary electron images showing the surface of NiO-YSZ layer in the three-layer MEAs.

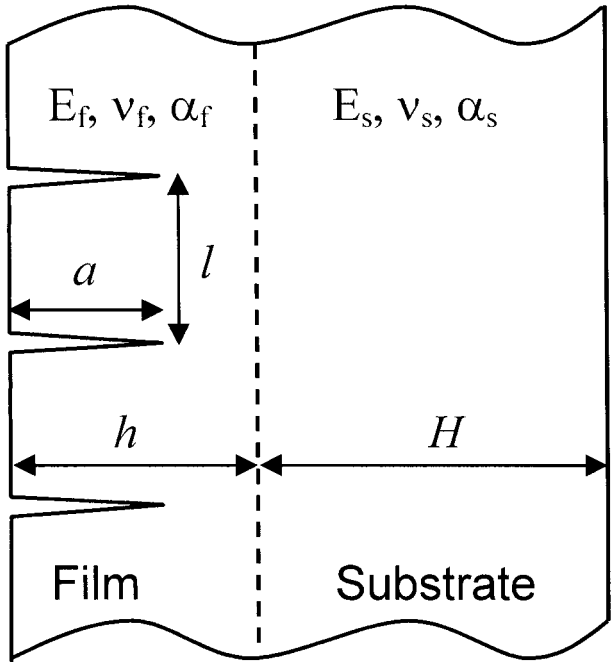

Figure 5 Schematic illustration of a thin coating with a series of semi-infinite and parallel cracks.

it propagates both towards the interface and laterally through the film. When the lateral crack length becomes a few times the film thickness, the energy release rate reaches a steady state value, G_{ch}, for propagation of the channel crack. Once $G_{ch} > \Gamma_f$, where Γ_f is the work of fracture of the coating, extensive channel cracking can occur in the coating layer. G_{ch} is related to the residual stress in the uncracked film, σ_f, and the film thickness, h, by [6]

$$G_{ch} = \omega_f \frac{\sigma_f^2 h}{E_f^*} \tag{6}$$

where $E_f^* = E_f/(1-\upsilon_f^2)$ is the plane strain modulus, E_f is the Young's modulus and ν_f is the Poisson's ratio of the film. ω_f is a non-dimensional function that depends on the Dundurs' parameters, α and β, and a/h described in Fig. 5. For plain strain conditions α and β are given by [8]

$$\alpha = \frac{E_f^* - E_s^*}{E_f^* + E_s^*} \tag{7}$$

and

$$\beta = \frac{\mu_f(1-2\nu_s) - \mu_s(1-2\nu_f)}{2\nu_f(1-2\nu_s) + 2\nu_s(1-2\nu_f)} \tag{8}$$

where the subscripts s and f denote the substrate and the film and μ is the shear modulus, $\mu = E/2(1+\nu)$. The Dundurs' parameters, α and β, for the anode MEAs take the values -0.62 and -0.27, respectively. The α and β values for the cathode MEAs are -0.73 and -0.25, respectively. The value of ω can be obtained from the analysis of Beuth [7]. Alternatively, for an analytical prediction of the thin film cracking behaviour, Beuth has shown that the function ω for the channel crack confined in the film (Fig. 5) can be calculated from

$$\omega_f = 3.951\frac{a}{h}\left(1-\frac{a}{h}\right)^{1-2s}\left(1+\lambda\frac{a}{h}\right)^2 \tag{9}$$

where a is the crack length, h is the thickness of the film (Fig. 5), s is the stress singularity exponent and λ is a fitting parameter to the numerical solution given in [9]. The stress singularity exponent s ($0< s <1$) is the root to

$$\cos(s\pi) - 2\left[\frac{\alpha-\beta}{1-\beta}\right](1-s)^2 + \left[\frac{\alpha-\beta^2}{1-\beta^2}\right] = 0 \tag{10}$$

Using the material parameters in Table I, $s = 0.33$ and $\lambda = 0.0627$ for the anode MEAs, and Equation 8 then gives $\omega_f = 1.47$ for a channel crack terminating at $a/h = 0.9$ in the anode layer. For a channel crack terminating at the interface ($a/h = 1.0$), we obtain $\omega_f = 1.36$ from the analysis of Beuth for $\alpha = -0.60$ and $\beta = \alpha/4$ which are close to those calculated for the anode MEAs. The channel crack analysis of Beuth [7] indicates that the crack growth in a film which is compliant with respect to the substrate will stop at a value of a/h close to, but less than 1. This should apply for the present analysis since the anode is much more compliant than the electrolyte. Hence, ω_f for $a/h = 0.9$ are reported here together with ω_f for $a/h = 1$.

If no cracking took place in the anode layer during cooling from the firing temperature, the residual stress for $\Delta T = 1100^\circ$C would be 66.5 MPa according to Equation 3. The fact that this value is greater than the fracture strength (56 MPa) is consistent with the channel cracking observed in the anode layer (Fig. 4). After channel cracking, the average residual stress drops down to 10.6 MPa (Table III). Hence, the fracture strength, 56 MPa, would be a good approximation for the initial stress, σ_f, in Equation 6 for the initiation of channel cracking. For partial cracking of the anode layer and $a/h = 0.9$ we thus obtain a work of fracture of $\Gamma_f = 2.84$ Jm^{-2}. For the cracks terminating at the interface the work of fracture becomes $\Gamma_f = 2.64$ Jm^{-2}. Similar calculations for channel cracking in the cathode layer give $\Gamma_f > 2.03$ Jm^{-2} for $a/h = 0.9$ and $\Gamma_f > 1.83$ Jm^{-2} for $a/h = 1.0$. These are minimum values since the residual stress (Table III) did not reach the fracture strength of the cathode (46 MPa) and channel cracking was not observed for the cathodes.

3.3. Biaxial flexure strength

The failure loads for the 3 different types of specimen are presented in Fig. 6 in Weibull format and the Weibull distribution parameters are given in Table IV. The strength of the electrolyte in the present experiments is very close to that of similar material reported earlier and given in Table I. The results show clearly that the anode has a negligible effect on the failure load, which is consistent with it having low residual stress, low elastic modulus and low strength. In contrast, the cathodes have a large weakening effect on the MEAs. In order to estimate the failure stress in

TABLE IV Weibull distribution parameters for the biaxial flexure loads of electrolyte and symmetrical MEAs

Specimen type	Mean failure load (N)	Weibull failure load (N)	Weibull modulus	Electrolyte stress at mean failure load (MPa)
YSZ	32.3	34.8	9.4	374.3
Anode MEA	35.1	38.7	6.8	343.1
Cathode MEA	14.0	15.9	2.3	182.0

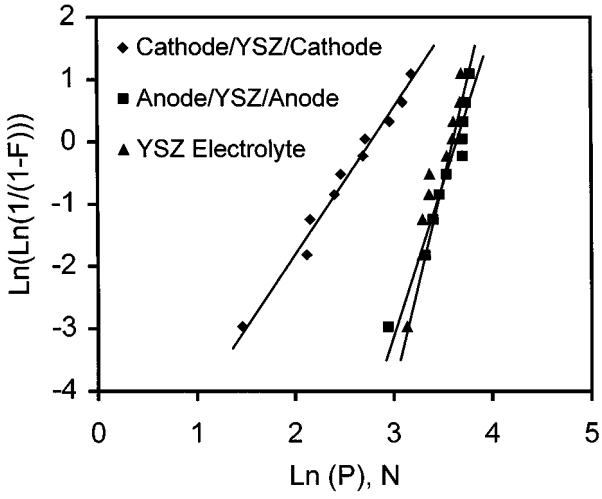

Figure 6 Weibull plots of biaxial failure loads for the YSZ electrolyte and the MEA specimens with symmetrical anode and cathode layers.

the electrolyte in the symmetrical MEAs the stress distribution (including the measured residual stress) was determined by finite element modelling (FEM) using the ABAQUS code. The resulting failure stresses are also given in Table IV and an example of the calculated stress distribution is shown in Fig. 7a. The Weibull plots based on the failure stresses of the electrolyte are shown in Fig. 8. These indicate that the stress in the YSZ at failure of the cathode MEAs is only approximately half that of the YSZ without electrodes. Furthermore the cathodes also reduce the Weibull modulus to a very low value, corresponding to a greater variability in failure load which is the sign of lower reliability.

Scanning electron microscopy (SEM) was used to study the fracture surfaces of the MEAs. The fracture of the anode symmetrical MEAs was accompanied by some delamination of the anode (Fig. 9a), the interface region has many large pores and there is only limited sintering of the anode to the electrolyte (Fig. 9b). The fracture surfaces indicated no evidence of the channel cracks in the anode penetrating into the electrolyte. Instead, the channel cracks are deflected by delamination. Fracture of the cathode symmetrical MEAs showed no sign of delamination (Fig. 10). The pores near the interface are much smaller and there is evidence of significant sintering between the cathode and the electrolyte. These observations are consistent with the higher residual stress observed in these specimens.

3.4. Effect of electrodes on strength

The behaviour of the symmetrical anode MEAs is straightforward to understand. The anode layer has no significant effect on the strength of the MEA specimens

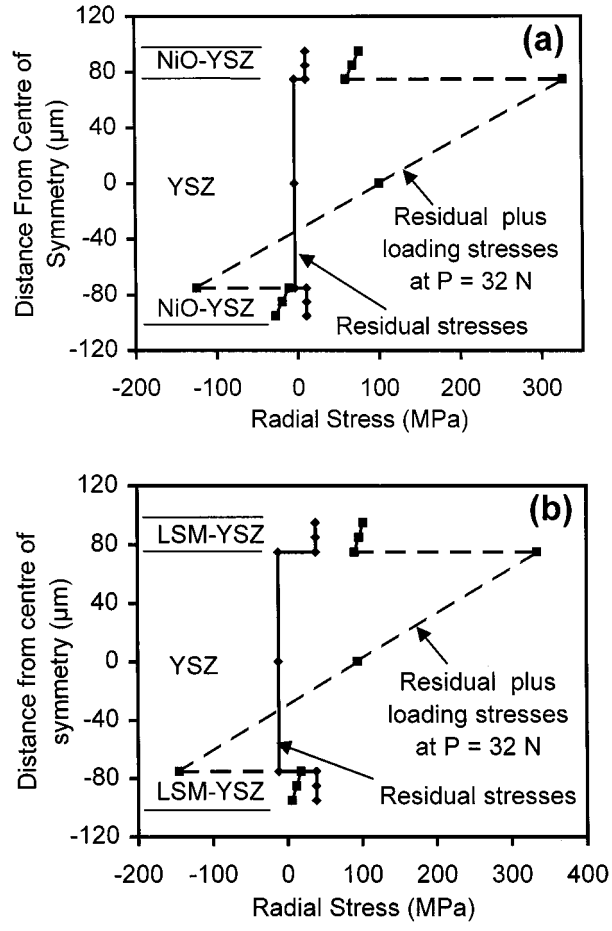

Figure 7 Variation of total stresses with position across the thickness of (a) the symmetrical anode MEA and (b) the symmetrical cathode MEA specimens at 25°C with no applied load (residual stresses only) and an applied load of 32 N in the biaxial flexure test.

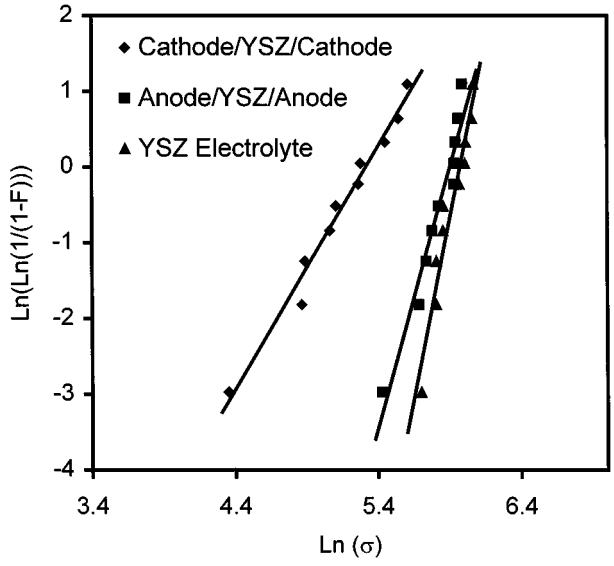

Figure 8 Weibull plots of biaxial failure stress for the YSZ electrolyte and the MEA specimens with symmetrical anode and cathode layers.

due to co-operative contributions from channel cracking during cooling from the firing temperature, ease of delamination at the anode-electrolyte interface and low residual stresses. Thus, the fractures of the anode and the electrolyte are two independent processes. (Although this situation has no unfavourable effect on the mechanical properties of the MEAs, delamination and

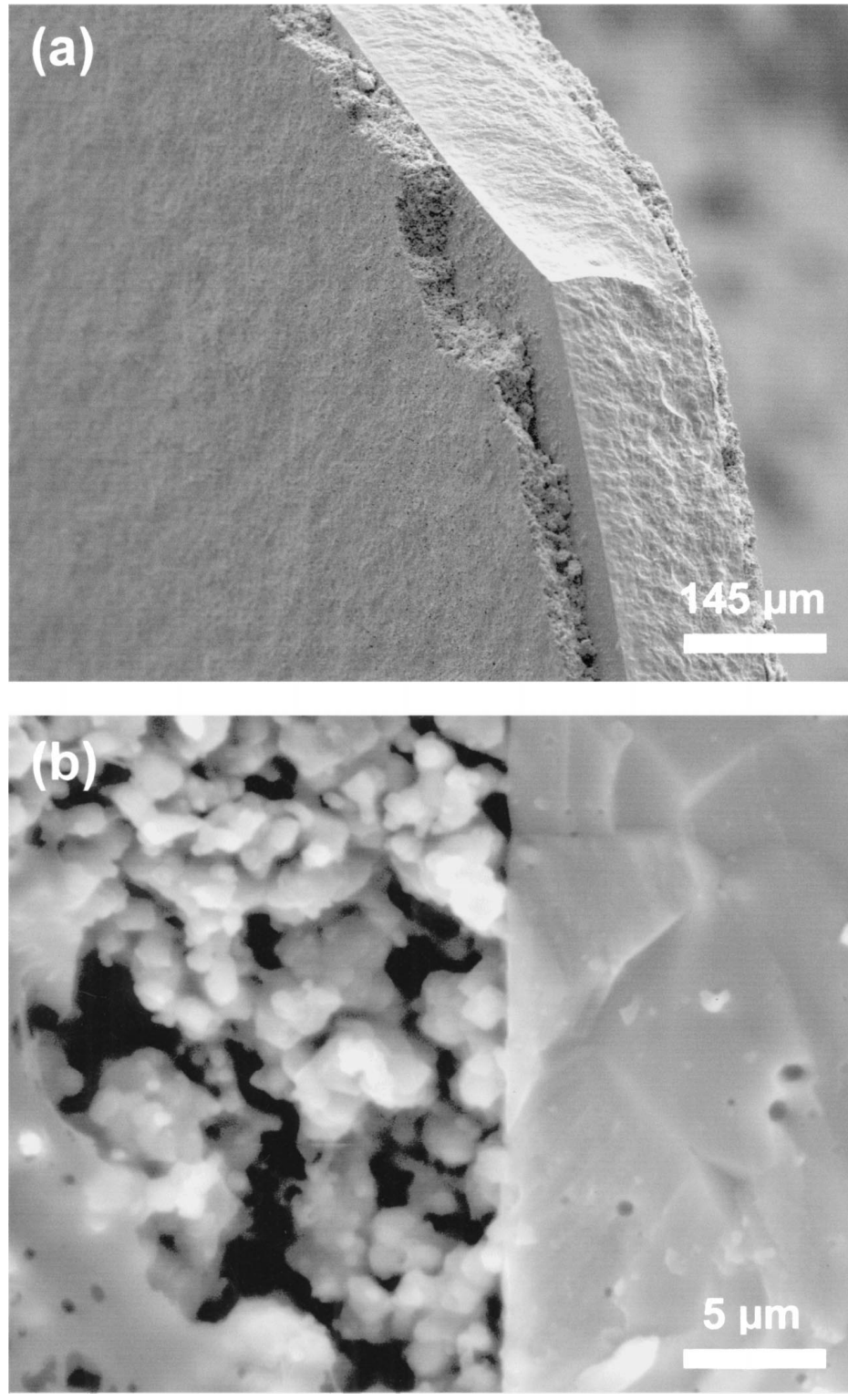

Figure 9 Scanning electron micrographs of fracture surfaces showing (a) the partial delamination of anode layer on the YSZ electrolyte and (b) the features in the interface region between the anode and electrolyte layers.

channel cracking will degrade the electrochemical performance of the SOFC.) Since the propagation of channel cracks from the anode into the electrolyte does not occur, the failure of the electrolyte requires the initiation of a crack from a defect in the electrolyte as observed for the YSZ electrolyte without the electrodes applied. These observations are consistent with the previous findings of Sorensen *et al*. [9] for the fracture of similar anode symmetrical MEAs sintered at 1200°C.

Conversely no noticeable channel cracking and delamination was observed in the symmetrical cathode MEAs. Higher residual stresses and better bonding at the cathode-electrolyte interface than those found for the anode seem to have a significant detrimental effect on the strength of the symmetrical cathode MEAs. However, the lowering of strength in the symmetrical cathode MEAs cannot be readily explained quantitatively. The tensile residual stress in the cathode is only 10 MPa less than its expected failure stress. Therefore, the cathode is not expected to support a much greater tensile stress during external loading. For example, according to the FEM results presented in Fig. 7b, the

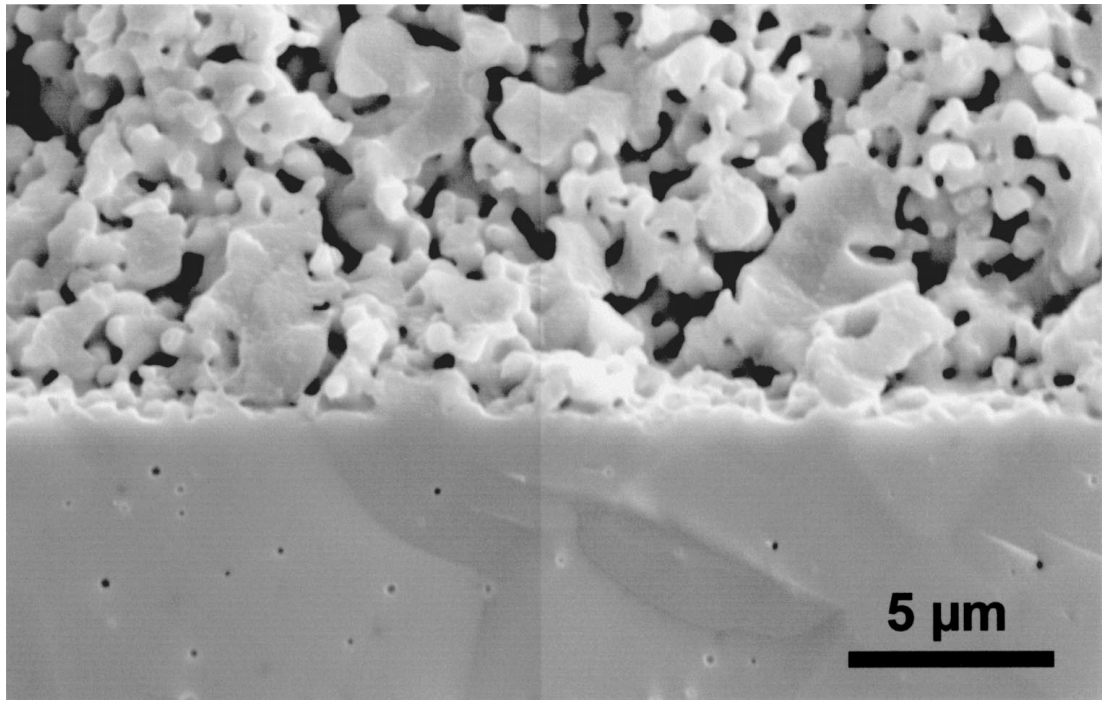

Figure 10 Scanning electron micrograph of the fracture surface of a symmetrical cathode MEA specimen, showing fine pores in the cathode section and the interface region indicating significant sintering between the cathode and the electrolyte.

tensile stress in the cathode surface is 103 MPa when the biaxial load applied to the MEA specimen reaches 32 N. Such a high tensile stress is unlikely to be achieved without fracture of the cathode.

Therefore, it is likely that a crack will form through the cathode early in biaxial loading and terminate at the interface with the electrolyte. Such a crack will give rise to an enhanced stress field in the electrolyte since delamination and crack deflection were shown not to occur (Fig. 10). Further increase in the applied biaxial load should lead to the penetration of the crack into the substrate before fracture. Alternatively, the crack tip may coincide with a defect on the electrolyte side of the interface so that the two cracks are superimposed to produce an enhanced stress field in the electrolyte.

Now, consider a cathode MEA specimen loaded in biaxial flexure. A number of cracks will be initiated in the cathode layer when the applied stress reaches the measured fracture strength of the cathode (46 MPa). As the applied load is increased, the crack tips will be driven toward the interface with the electrolyte. The crack tips will stop at the interface (Fig. 11a) and will not penetrate into the electrolyte until the stress in the electrolyte, σ_s, exceeds a critical value, σ_c (Fig. 11b). For this condition, assuming that the crack tip has a square-root stress singularity, the stress intensity factor, K_s, for propagation of a crack into the substrate can be defined by the Equation 7

$$K_s = (h\omega_f)^{1/2}\sigma_{fs} \tag{11}$$

where σ_{fs} is the fracture strength of the film (the cathode).

When $\sigma_s \geq \sigma_c$, the crack will penetrate into the electrolyte by a distance, a_s, as shown in Fig. 11b. Also the crack in the cathode may coincide with a flaw located on the electrolyte side of the interface. In both cases, the

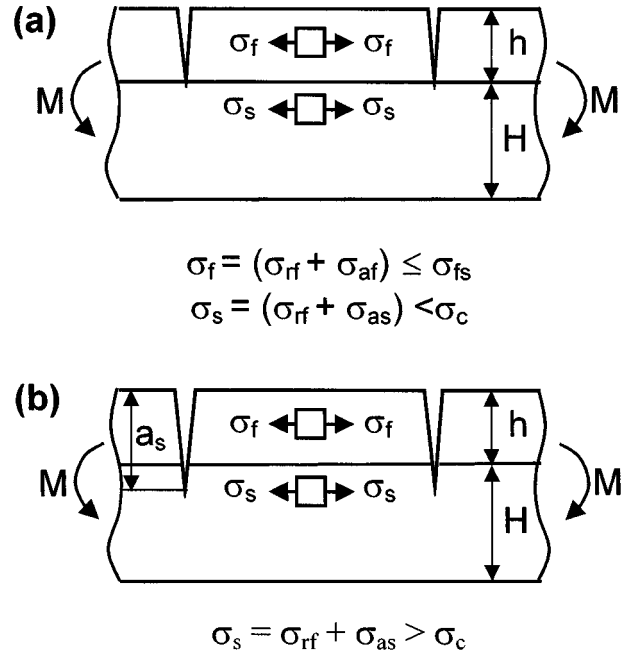

Figure 11 Schematic illustration of (a) a crack in the film extended to the interface to the substrate and (b) a crack penetrated into the substrate. The bilayer structure in both conditions is under the influence of residual and bending stresses.

stress intensity at the crack tip results from the superimposition of the residual and applied stresses. Hence, the principle of superposition leads to

$$K_I = K_s + K_{as} \tag{12}$$

where K_s is given in Equation 11 and K_{as} is the stress intensity factor for a crack on the electrolyte side of the interface under the applied stress, σ_{as}, defined in Fig. 11b.

Analogous to our previous stress analysis for a surface crack in the electrolyte [3], the stress intensity

factor, K_{as}, can be defined by the equation

$$K_{as} = Y\sigma_{as}(\pi(a_s - h))^{1/2} \quad (13)$$

where Y is a correction factor for the geometry of the crack and a_s and h are defined in Fig. 11. Combining Equations 11, 12 and 13 gives

$$K_I = (h\omega_f)^{1/2}\sigma_{fs} + Y\sigma_{as}(\pi(a_s - h))^{1/2} \quad (14)$$

It should be noted that Equation 14 is an approximate solution for K_I because the stress singularity dependence of K_s, has been assumed to have an exponent $s = 0.5$ whereas the value of s is $\sim$0.33 for the present crack problem.

We have shown previously [3] that, for similar YSZ electrolytes, the flexural strength is controlled by surface flaws of a size in the range from 7 to 35 μm and the fracture toughness is 1.6 MPa $m^{1/2}$ at room temperature. Assuming that the critical flaw size for the electrolyte is 10 μm for which we found $Y = 0.76$ [10] and $K_{IC} = 1.6$ MPa $m^{1/2}$, Equation 13 predicts an electrolyte strength of $\sigma_{as} = 347$ MPa. This is close to the measured strength, 374 MPa (Table IV), indicating that the critical defect size for the electrolyte specimens is approximately 10 μm.

Now consider a cathode MEA specimen under a biaxial flexure stress, which has resulted in extensive cracking of the cathode layer, and at least one of the cracks coincides with a 10 μm deep flaw on the electrolyte side of the interface. For this condition, taking $\omega_f = 1.28$ and $Y = 0.82$ determined from the analyses in [7] and [10] respectively, together with $K_{IC} = 1.6$ MPa $m^{1/2}$ and $\sigma_{fs} = 46$ MPa (Table I), we estimate $\sigma_{as} = 300$ MPa for the fracture of a cathode MEA specimen from Equation 14. This is much higher than the average measured strength, 182 MPa (Table IV). Repeating the same calculations for a flaw size of 45 μm gives $\sigma_{as} = 197$ MPa, which is close to the measured strength. However fracture initiation in the electrolyte layer from a 45 μm deep flaw could not be confirmed by the SEM investigations of the fracture surfaces because the specimens broke into several pieces due to crack branching during unstable crack propagation. Therefore, it is not clear whether such large defects were responsible for lowering the strength of the MEAs.

The fracture analysis used here is not exact and approximations have been made in estimating the stress intensity at a flaw in the electrolyte which coincides with a channelling crack in the electrode. These include assuming a common exponent for the stress singularities; assuming that the stress intensity of the two dimensional channelling crack can be added directly to that of a three dimensional flaw in the electrolyte; and limiting the maximum stress in the electrode to the fracture strength of bulk specimens of the electrode material. Nevertheless, the discrepancy between the observed strength of the cathode MEAs and the calculated strength is too large to be accounted for by errors arising from these assumptions. It is therefore inferred that processing the cathodes has damaged the electrolyte in some way so as to enlarge the size of electrolyte defects or/and reduce the fracture toughness of the electrolyte near the interface. For example, there might be some diffusion of Mn from the cathode into the electrolyte, but the A-site deficient composition of the cathode material employed in this work should prevent the formation of $La_2Mn_2O_7$ [11]. However, there is as yet no direct evidence for either of these explanations.

4. Conclusions

The residual stress in screen printed SOFC anodes is very low (11 MPa) due to stress relief by extensive channel cracking on cooling since the thermoelastic cooling stress exceeds the strength of the anode. The residual stress in the cathodes is much higher (39 MPa) and is in reasonable agreement with that expected from elastic deformation caused by thermal expansion mismatch on cooling from the fabrication temperature.

The applied load at failure, and the stress in the electrolyte at failure (343 MPa), for symmetrical anode MEAs are almost equal to those of the unelectroded electrolyte plates (374 MPa). This is consistent with the low residual stress and observed crack deflection by delamination at the anode/electrolyte interface.

The applied load at failure, and the stress in the electrolyte at failure (182 MPa), for symmetrical cathode MEAs are much lower than those of the unelectroded electrolyte plates. This is partially explained by the residual stress in the cathode acting to increase the applied stress intensity at defects in the electrolyte. However, this effect is not large enough to explain quantitatively the reduced strength of cathode MEAs.

Acknowledgements

The authors are particularly grateful to Dr. W. Kleinlein (Siemens, Germany) for the provision of specimens and helpful discussions. The research described was carried out with financial support from European Union project JOE3-CT95-0015.

References

1. A. SELÇUK and A. ATKINSON, *J. Eur. Ceram. Soc.* **17** (1997) 1523.
2. A. ATKINSON and A. SELÇUK, in Proceedings of the Fifth International Symposium on Solid Oxide Fuel Cells, edited by U. Stimming, S. C. Singhal, H. Tagawa and W. Lehnert (Electrochemical Society Proceedings 1997) Vol. 97–40, p. 671.
3. A. SELÇUK and A. ATKINSON, *J. Am. Ceram. Soc.* **83** (2000) 2029.
4. A. ATKINSON and A. SELÇUK, in Proceedings of the Third European Solid Oxide Fuel Cell Forum Vol 1, Nantes, edited by P. Stevens and U. Bossel (Oberrohrdorf, Switzerland, 1998) p. 343.
5. C. H. HSUEH and A. G. EVANS, *J. Am. Ceram. Soc.* **68** (1985) 241.
6. T. YE, Z. SUO and A. G. EVANS, *Int. J. Solids and Struct.* **29** (1992) 2639.
7. J. L. BEUTH, *Int. J. Solids and Struct.* **29** (1992) 1657.
8. J. DUNDURS, *J. App. Mech.* **36** (1969) 650.
9. B. F. SORENSEN and S. PRIMDAHL, *J. Mater. Sci.* **33** (1998) 5291.
10. J. C. NEWMAN and I. S. RAJU, *Eng. Fract. Mech.* **15** (1981) 185.
11. J. A. M. VAN ROOSMALEN and E. H. P. CORDFUNKE, *Solid State Ionics* **52** (1992) 303.

Received 26 May
and accepted 27 June 2000